A continuum thermodynamics model for the sensing effect in ferromagnetic shape memory Ni–Mn–Ga

N. N. Sarawate and M. J. Dapino[a)]
Department of Mechanical Engineering, The Ohio State University, Columbus, Ohio 43210

(Received 12 July 2006; accepted 6 May 2007; published online 26 June 2007)

A magnetomechanical model based on continuum thermodynamics is presented which describes the sensing effect in single-crystal ferromagnetic shape memory Ni–Mn–Ga. The model quantifies the stress and magnetization dependence on strain at different values of bias fields under isothermal conditions. A magnetic Gibbs energy is considered as the thermodynamic potential with Zeeman, magnetostatic, and anisotropy energy contributions. Constitutive equations for stress and magnetization are obtained in the isothermal case after restricting the process through the Clausius-Duhem inequality for the second law of thermodynamics. Mechanical dissipation and the microstructure of Ni–Mn–Ga are incorporated in the continuum model through the internal state variables volume fraction, domain fraction, and magnetization rotation angle. Closed-form solutions describing the evolution of the internal state variables are developed. The model requires only seven parameters identified from simple experiments: stress-strain curve at zero field, and easy-axis and hard-axis magnetization curves. © *2007 American Institute of Physics*. [DOI: 10.1063/1.2748356]

I. INTRODUCTION

Ferromagnetic shape memory alloys (FSMAs) generate large strains (typically 6% in Ni–Mn–Ga) in response to magnetic fields of approximately 700 kA/m.[1] These materials exhibit heat-induced martensite to austenite transformation and magnetic field-induced strain (MFIS) by twin variant rearrangement in the low temperature martensite phase. Applications for Ni–Mn–Ga are primarily based on the latter. The advantage of FSMAs over conventional shape memory materials lies in the faster response provided by the magnetic field application,[2] which combined with the large strains, makes FSMAs potentially attractive for actuation applications.

The effect of magnetic field on strain, or actuator effect, has been extensively characterized and modeled (see, e.g., review papers[3,4]). However, the effect of external mechanical input on the magnetic behavior of Ni–Mn–Ga, or sensor effect, has received only limited attention. Mullner *et al.*[5] experimentally studied strain-induced changes in the flux density of single-crystal $Ni_{51}Mn_{28}Ga_{21}$ under external quasistatic loading at a constant field of 558 kA/m. Straka and Heczko[6] reported on the superelastic response of single-crystal $Ni_{49.7}Mn_{29.1}Ga_{21.2}$ with 5 M martensitic structure for fields higher than 239 kA/m, and established the interconnection between magnetization and strain. Heczko[7] further investigated this interconnection and proposed a simple energy model. Li *et al.*[8] reported the effect of magnetic field during martensitic transformation on the magnetic and elastic behavior of $Ni_{50.3}Mn_{28.7}Ga_{21}$. Suorsa *et al.*[9] reported magnetization measurements conducted on stoichiometric Ni_2MnGa material for various discrete strain and field intensities ranging between 0% and 6% and 5 and 120 kA/m, respectively. Sarawate and Dapino[10] experimentally characterized flux density as a function of strain loading and unloading at various fixed magnetic fields for commercial Ni–Mn–Ga single crystal. From these measurements, the bias field needed for maximum recoverable flux density change was determined. This bias field was shown to mark the transition from irreversible (quasiplastic) to reversible (pseudoelastic) stress-strain behavior. A reversible flux density change of 145 mT was observed over a range of 5.8% strain and 4.4 MPa stress at a bias field of 368 kA/m, thus suggesting the use of Ni–Mn–Ga as a high-compliance, high-displacement deformation sensor.

This paper presents a thermodynamic model which describes the sensing behaviors characterized by Sarawate and Dapino.[10] Several models have been proposed for describing twin variant rearrangement in FSMAs, with the primary intent of characterizing the MFIS or actuator behavior. An early model by O'Handley[11] quantifies the strain and magnetization dependence on field by energy minimization. The contributions of elastic, Zeeman, and anisotropy energy were considered, with the latter defining three cases depending on its strength being low, medium, or high. Glatavaska *et al.*[12] developed a statistical model for MFIS by relating the ferromagnetic magnetoelastic interactions to the internal microstress in the martensite. Chernenko *et al.*[13] further modified this model to describe in detail the quasiplastic and superelastic stress-strain response of FSMAs at varied bias fields.

Likhachev and Ullakko[14] presented a model where the easy-axis and hard-axis magnetic energy difference was considered as the magnetic field-induced driving force acting on a twin boundary. The magnetization was assumed to be a linear combination of easy-axis and hard-axis magnetization values related by the volume fraction. A similar model was utilized by Straka and Heczko[6] for describing the stress-strain response at varied bias fields. A model by Couch and Chopra[15] was based on an approach similar to that by Brinson[16] for shape memory materials, where the stress was

a)Author to whom correspondence should be addressed; electronic mail: dapino.1@osu.edu

assumed to be a linear combination of strain, volume fraction, and magnetic field. While this model is tractable, the identification of model parameters requires stress-strain testing over a range of bias fields in order to obtain the necessary stress profiles as a function of field.

Hirsinger and Lexcellent[17,18] presented a thermodynamic model in which the microstructure of single-crystal Ni–Mn–Ga was represented by internal state variables, and evolution of these variables was used to quantify the strain and magnetization response to applied magnetic fields. The anisotropy energy effect was not considered in Ref. 17 but was later considered in Ref. 18 in order to model the magnetization. Kiefer and Lagoudas[19] employed a similar approach with a more detailed thermodynamics treatment. Polynomial and trigonometric hardening functions were introduced to account for interaction of evolving volume fractions. However, this leads to more parameters in the model. Faidley *et al.*[20] constructed the Gibbs energy potential for the case when the twin boundaries are pinned by dislocations, which had been previously shown by Malla *et al.*[21] to allow in some cases for reversible twin boundary bowing when the single crystal is driven with a collinear magnetic field and stress pair. While similar in concept to the models for MFIS by Hirsinger and Lexcellent[17] and Kiefer and Lagoudas,[19] in this model the energy of a mechanical spring is added to the Zeeman and elastic energies to account for the internal restoring force supplied by the pinning sites. The anisotropy energy was assumed to be infinite in Refs. 19 and 20 and magnetostatic energy was not considered with the argument that it depends on the geometry of a sample. One tenet of the proposed model is that the magnetostatic energy is an important component of the magnetization response, which is critical for the sensing effect. The magnetostatic energy is thus considered as a means to quantify the demagnetization field in the continuum. While the magnitude of the demagnetization field depends on a specimen's shape, it can be assumed to be uniform throughout a continuum.

The thermodynamic framework in this paper is similar to that in Refs. 17, 19, and 20. However, the focus is on modeling the sensing behavior and magnetic field induced pseudoelasticity in FSMAs. The outline of the paper is as follows. A brief thermodynamic background with the inclusion of magnetic terms is given in Sec. II. The incorporation of the Ni–Mn–Ga microstructure in the continuum thermodynamics framework using the internal state variables volume fraction, domain fraction, and magnetization rotation angle is discussed in Sec. III. In Sec. IV, a specific form of thermodynamic potential termed magnetic Gibbs energy is defined which includes Zeeman, magnetostatic, and anisotropy energy contributions. The mechanical energy includes an elastic component and a disspative component due to detwinning. As is often done for modeling of shape memory alloys, we decompose the total strain into an elastic and detwinning strain. The process associated with magnetization variables is assumed to be reversible but the evolution of volume fractions is assumed to be dissipative, which implies that the constitutive response depends on the volume fraction history. The internal state variables associated with the magnetization parameters evolve along with the variant volume fraction, which results in interesting magnetomechanical behaviors. The evolution of magnetic parameters and volume fraction are discussed in Secs. V and VI, respectively. The model requires only seven parameters, which are determined through the following simple experiments: stress-strain curve at zero bias field, and easy-axis and hard-axis magnetization curves. A comparison of model results with experimental measurements is presented in Sec. VII.

II. THERMODYNAMIC FRAMEWORK

The law of conservation of energy dictates that the rate of change of internal energy of any part S of a body is equal to the rate of mechanical work of the net external force acting on S plus all other energies that enter or leave S. In local form, the conservation law has the form

$$\rho\dot{\epsilon} = \mathbf{T}\cdot\mathbf{D} + \mu_0\mathbf{H}\cdot\dot{\mathbf{M}} + \rho r - \operatorname{div}\mathbf{q}, \tag{1}$$

where ϵ is the internal energy, ρ is the density of the material, $\mathbf{T}$ is the Cauchy stress tensor, $\mathbf{D}$ is the deformation rate tensor, r is the heat source inside the system, and $\mathbf{q}$ is a heat flux vector representing the heat going out of the system. The term $\mathbf{T}\cdot\mathbf{D}$ represents the stress power due to external mechanical action. The term $\mu_0\mathbf{H}\cdot\mathbf{M}$ represents the energy supplied to the material by a magnetic field,[22] with $\mathbf{H}$ denoting the resultant applied magnetic field vector and $\mathbf{M}$ the net magnetization vector inside the material. For the one-dimensional case under consideration, in which the externally applied strain ε and engineering stress σ are oriented along the longitudinal axis of the sample, Eq. (1) reduces to

$$\rho\dot{\epsilon} = \sigma\dot{\varepsilon} + \mu_0\mathbf{H}\cdot\dot{\mathbf{M}} + \rho r - \operatorname{div}\mathbf{q}. \tag{2}$$

The Clausius-Duhem inequality states that the rate of change of entropy is greater than or equal to the entropy increase rate due to the specific heat supply rate minus the entropy decrease rate due to the heat flux vector. Mathematically, this is expressed in local form as

$$\rho\dot{\eta} \geqslant \rho\frac{r}{\Theta} - \operatorname{div}\left(\frac{\mathbf{q}}{\Theta}\right), \tag{3}$$

where Θ is the absolute temperature, and η is specific entropy.

Elimination of r from (2) and (3) gives

$$\rho\Theta\dot{\eta} - \rho\dot{\epsilon} + \sigma\dot{\varepsilon} + \mu_0\mathbf{H}\cdot\dot{\mathbf{M}} - \frac{1}{\Theta}\mathbf{q}\cdot\operatorname{grad}\Theta \geqslant 0. \tag{4}$$

The thermomagnetomechanical material involved in the above expressions has the constitutive dependencies

$$\begin{aligned}\epsilon &= \epsilon(\varepsilon,\mathbf{M},\eta),\\ \sigma &= \sigma(\varepsilon,\mathbf{M},\eta),\\ \mathbf{H} &= \mathbf{H}(\varepsilon,\mathbf{M},\eta).\end{aligned} \tag{5}$$

Because the temperature Θ is easier to control in characterization of thermoelastic materials, it is usual practice to use it as the independent variable and the Helmholtz energy as the potential, rather than the entropy and internal energy. The Legendre transformation provides a relation between the internal energy and the Helmholtz free energy ψ,

$$\psi = \epsilon - \Theta\eta, \tag{6}$$

which in combination with the Clausius-Duhem inequality (4) gives

$$\rho\dot{\psi} - \rho\eta\dot{\Theta} + \sigma\dot{\varepsilon} + \mu_0 H\dot{M} - \frac{1}{\Theta}\mathbf{q}\cdot\text{grad}\,\Theta \geq 0, \tag{7}$$

with M the magnitude of magnetization in the direction of applied field H. The constitutive dependencies are

$$\begin{aligned}\psi &= \psi(\varepsilon, M, \Theta, \text{grad}\,\Theta)\\ \sigma &= \sigma(\varepsilon, M, \Theta, \text{grad}\,\Theta)\\ H &= H(\varepsilon, M, \Theta, \text{grad}\,\Theta).\end{aligned} \tag{8}$$

Assuming isothermal processes, $\dot{\Theta}=0$ and grad $\Theta=0$, inequality (7) becomes

$$-\rho\dot{\psi} + \sigma\dot{\varepsilon} + \mu_0 H\dot{M} \geq 0, \tag{9}$$

also implying that the absolute temperature and its gradient can be eliminated as independent variables in (8). Once the specific form of Helmholtz free energy is defined, the Clausius-Duhem inequality (9) can be used to arrive at the constitutive response of the system.

III. INCORPORATION OF THE Ni–Mn–Ga MICROSTRUCTURE IN THE THERMODYNAMIC FRAMEWORK

The framework discussed in Sec. II pertains to thermomagnetomechanical materials which have a perfect memory of their reference configuration and temperature. Like shape memory materials, FSMAs have imperfect memory, i.e., the materials when loaded and unloaded do not necessarily return to their initial undeformed configuration and temperature. Internal state variables allow one to extend the results of thermoelastic theory to dissipative materials and account for certain microstructural phenomena. In our approach, the internal state variable volume fraction ξ accounts for mechanical dissipation. The three internal state variables volume fraction ξ, domain fraction α, and magnetization rotation angle θ are used to incorporate the magnetomechanical microstructure into the continuum model.

A simplified two-variant microstructure is shown in Fig. 1, where the applied field is oriented in the x direction, and the applied stress (or strain) is oriented in the y direction. This microstructure is motivated from experimental observations of single-crystal Ni–Mn–Ga.[23] A field-preferred variant, with volume fraction ξ, is one in which the crystallographic easy c axis is aligned with the x direction. A stress-preferred variant, with volume fraction $1-\xi$, is one in which the c axis is oriented in the y direction. It is assumed that the variant volume fractions are sufficiently large to be subdivided into

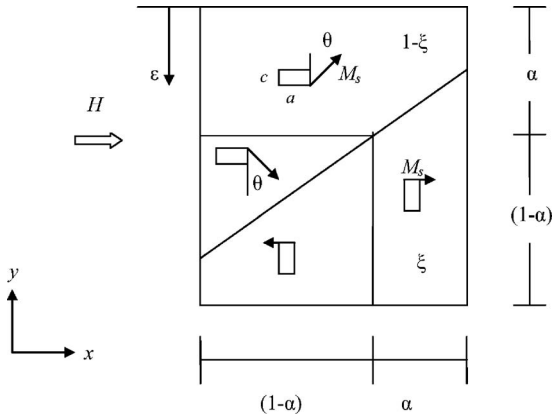

FIG. 1. (Color online) Simplified twin variant microstructure of Ni–Mn–Ga.

180° magnetic domains with volume fractions α and $1-\alpha$. This domain structure minimizes the net magnetostatic energy due to finite dimensions of the sample. In the absence of an external field, the domain fraction $\alpha=1/2$ will lead to minimum magnetostatic energy. For an arbitrarily oriented specimen, the magnetization vector is not always parallel to the easy c axis due to the competition between the spin-orbit and magnetic dipole interactions.[24] Ignoring these effects, the high magnetocrystalline energy of Ni–Mn–Ga dictates that the magnetization vectors in a field-preferred variant are attached to the crystallographic c axis, i.e., they are oriented in the direction of the applied field or in the opposite direction. Any rotation of the magnetization vectors away from the c axis results in an increase in the anisotropy energy. The magnetization vectors in a stress-preferred variant are oriented at an angle θ relative to the c axis. Energy minimization dictates that this angle is equal and opposite in the two magnetic domains within a stress-preferred variant.

The magnetization component in the x direction can thus be written as

$$\begin{aligned}M(\xi,\alpha,\theta) &= M_s[\xi\alpha - \xi(1-\alpha) + (1-\xi)\alpha\sin\theta\\ &\quad + (1-\xi)(1-\alpha)\sin\theta]\\ &= M_s[2\xi\alpha - \xi + \sin\theta - \xi\sin\theta],\end{aligned} \tag{10}$$

in which M_s denotes the saturation magnetization.

In the system with constitutive dependencies (8), the magnetization component M is an independent variable. For the sensor under consideration, it is desired to have the external magnetic field H as an independent variable instead of M. A thermodynamic potential termed magnetic Gibbs energy ϕ is thus obtained through the Legendre transformation

$$\rho\phi = \rho\psi - \mu_0 HM. \tag{11}$$

Therefore,

$$\rho\dot{\psi} = \rho\dot{\phi} + \mu_0 M\dot{H} + \mu_0 H\dot{M}. \tag{12}$$

Substitution of $\rho\dot{\psi}$ in Eq. (9) gives a modified form of the Clausius-Duhem inequality,

$$-\rho\dot{\phi} + \sigma\dot{\varepsilon} - \mu_0 M\dot{H} \geq 0, \tag{13}$$

which defines a thermomagnetomechanical material with the following constitutive dependencies:

$$\phi = \phi(\varepsilon, H, \xi, \alpha, \theta),$$

$$\sigma = \sigma(\varepsilon, H, \xi, \alpha, \theta), \tag{14}$$

$$M = M(\varepsilon, H, \xi, \alpha, \theta).$$

Application of the chain rule yields

$$\rho\dot{\phi}(\varepsilon, H, \xi, \alpha, \theta) = \frac{\partial(\rho\phi)}{\partial\varepsilon}\dot{\varepsilon} + \frac{\partial(\rho\phi)}{\partial H}\dot{H} + \frac{\partial(\rho\phi)}{\partial\alpha}\dot{\alpha} + \frac{\partial(\rho\phi)}{\partial\xi}\dot{\xi} + \frac{\partial(\rho\phi)}{\partial\theta}\dot{\theta}. \tag{15}$$

Substitution of relation (15) in the Clausius-Duhem inequality (13) gives

$$-\left[\frac{\partial(\rho\phi)}{\partial\varepsilon}\dot{\varepsilon} + \frac{\partial(\rho\phi)}{\partial H}\dot{H} + \frac{\partial(\rho\phi)}{\partial\alpha}\dot{\alpha} + \frac{\partial(\rho\phi)}{\partial\xi}\dot{\xi} + \frac{\partial(\rho\phi)}{\partial\theta}\dot{\theta}\right] + \sigma\dot{\varepsilon} - \mu_0 M\dot{H} \geqslant 0, \tag{16}$$

which can be expanded as follows:

$$\left[\sigma - \frac{\partial(\rho\phi)}{\partial\varepsilon}\right]\dot{\varepsilon} + \left[-\mu_0 M - \frac{\partial(\rho\phi)}{\partial H}\right]\dot{H} + \pi^{\alpha}\dot{\alpha} + \pi^{\theta}\dot{\theta} + \pi^{\xi}\dot{\xi} \geqslant 0 \tag{17}$$

in which the terms $\pi^{\alpha} = -\partial(\rho\phi)/\partial\alpha$, $\pi^{\theta} = -\partial(\rho\phi)/\partial\theta$, and $\pi^{\xi} = -\partial(\rho\phi)/\partial\xi$ represent thermodynamic driving forces associated with internal state variables α, θ, and ξ, respectively. In Eq. (17), the terms $\dot{\varepsilon}$ and $\dot{H}$ are independent of each other, and of other rates. Therefore, for an arbitrary process, the coefficients of $\dot{\varepsilon}$ and $\dot{H}$ must vanish in order for the inequality to hold. This leads to the constitutive equations

$$\sigma = \frac{\partial(\rho\phi)}{\partial\varepsilon}, \tag{18}$$

$$M = -\frac{1}{\mu_0}\frac{\partial(\rho\phi)}{\partial H}. \tag{19}$$

The Clausius-Duhem inequality thus takes the reduced form

$$\pi^{\alpha}\dot{\alpha} + \pi^{\theta}\dot{\theta} + \pi^{\xi}\dot{\xi} \geqslant 0. \tag{20}$$

IV. ENERGY FORMULATION

A. Magnetic energy

The total magnetic energy of a Ni–Mn–Ga sensor includes Zeeman, magnetostatic, and magnetocrystalline anisotropy contributions. The Zeeman energy, which represents the energy available to drive the motion of twin boundaries by magnetic fields, is minimum when the magnetization vectors are completely aligned in the direction of the externally applied field, and is maximum when the magnetization vectors are aligned in the direction opposite to the externally applied field. For the simplified two-variant system shown in Fig. 1 with net magnetization component M in the direction of externally applied field H, the Zeeman energy has the form

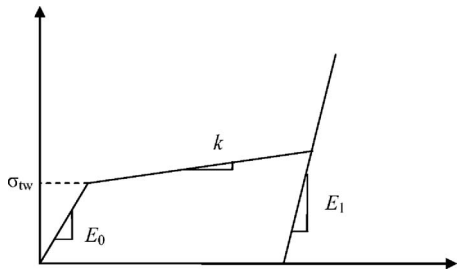

FIG. 2. (Color online) Schematic of stress-strain curve at zero bias field.

$$\rho\phi_{\mathrm{ze}}(H, \xi, \alpha, \theta) = -\mu_0 M_s(2\xi\alpha - \xi + \sin\theta - \xi\sin\theta)H. \tag{21}$$

The magnetization creates a demagnetization field which opposes the externally applied magnetic field and depends on sample geometry. For the system shown in Fig. 1, the magnetostatic energy which quantifies the demagnetization is given by

$$\rho\phi_{\mathrm{ms}}(\xi, \alpha, \theta) = \frac{1}{2}\mu_0 N M_s^2(2\xi\alpha - \xi + \sin\theta - \xi\sin\theta)^2, \tag{22}$$

where N represents the difference in the demagnetization factors along the x and y directions.[25]

The magnetocrystalline anisotropy energy represents the energy needed to rotate a magnetization vector away from the easy c axis. This energy is minimum (or zero) when the magnetization vectors are aligned along the c axis and is maximum when they are rotated 90° away from the c axis. In Fig. 1, all the contribution towards the anisotropy energy comes from the stress preferred variant. The anisotropy energy is thus given by

$$\rho\phi_{\mathrm{an}}(\xi, \alpha, \theta) = K_u(1 - \xi)\sin^2\theta. \tag{23}$$

The anisotropy constant, K_u, is calculated experimentally as the difference in the area under the easy-axis and hard-axis magnetization curves. It represents the energy associated with pure rotation of the magnetization vectors (hard axis) compared to the magnetization due to zero rotation of vectors (easy axis). In this case, it has the value 1.675×10^5 J/m^3.[10]

The total magnetic energy is written as the sum of expressions (21)–(23),

$$\rho\phi_{\mathrm{mag}}(H, \xi, \alpha, \theta) = -\mu_0 M_s(2\xi\alpha - \xi + \sin\theta - \xi\sin\theta)H + \frac{1}{2}\mu_0 N M_s^2(2\xi\alpha - \xi + \sin\theta - \xi\sin\theta)^2 + K_u(1 - \xi)\sin^2\theta. \tag{24}$$

B. Mechanical energy

The model parameters required for determination of the mechanical energy of the system are obtained from the stress-strain plot at zero bias field (Fig. 2). The material is compressed from its longest length ($\xi = 1$) to beyond the length corresponding to complete stress-preferred variant state ($\xi = 0$). The total strain is considered to be composed of an elastic and a detwinning component,[12,13,16,26]

$$\varepsilon = \varepsilon_e + \varepsilon_{\mathrm{tw}}. \tag{25}$$

The elastic strain and total stress are related by effective modulus $E(\xi)$; the detwinning strain and total stress are related by parameter $a(\xi)$. The mechanical energy contribution to the magnetic Gibbs energy thus has the form

$$\rho\phi_{\mathrm{mech}}(\varepsilon,\xi) = \frac{1}{2}E(\xi)\varepsilon_e^2 + \frac{1}{2}a(\xi)\varepsilon_{\mathrm{tw}}^2. \tag{26}$$

The detwinning strain is assumed to be linearly proportional to the stress-preferred volume fraction,

$$\varepsilon_{\mathrm{tw}} = \varepsilon_0(1-\xi), \tag{27}$$

with ε_0 the maximum detwinning strain $(1-c/a)$. Combination of (25) and (27) results in the following expression for the elastic strain:

$$\varepsilon_e = \varepsilon - \varepsilon_0(1-\xi). \tag{28}$$

The slope of the stress-strain plot in the detwinning region is denoted by k. Assuming that the detwinning region includes both detwinning and elastic strain components, k is represented by two springs in series,

$$\frac{1}{k} = \frac{1}{a(\xi)} + \frac{1}{E(\xi)}. \tag{29}$$

Experimentally, it is observed that the initial modulus of the sample, E_0, is significantly lower than that in fully compressed state, E_1. Denoting S_0 and S_1 the respective compliances, the intermediate compliance $S(\xi)$ is formulated as done in certain cases for shape memory materials by assuming a linear combination of the two extreme values. Thus the effective modulus is given by the expression

$$E(\xi) = \frac{1}{S(\xi)} = \frac{1}{S_0 + (1-\xi)(S_1 - S_0)}. \tag{30}$$

The parameters have the numerical values, $k=16$ MPa, $E_0=400$ MPa, and $E_1=3000$ MPa.[10]

When the sample is compressed, the initial high modulus region is followed by the low modulus detwinning region. The stress value at the onset of detwinning at zero magnetic field, σ_{tw}, is a model parameter. The detwinning stress is observed to increase with increasing bias field. Combining relations (26)–(30), the mechanical energy takes the form

$$\rho\phi_{\mathrm{mech}}(\varepsilon,\xi) = \frac{1}{2}[S_0 + (1-\xi)(S_1-S_0)]^{-1}[\varepsilon - \varepsilon_0(1-\xi)]^2 + \frac{1}{2}\{k^{-1} - [S_0 + (1-\xi)(S_1-S_0)]\}^{-1}\varepsilon_0^2(1-\xi)^2. \tag{31}$$

The total free energy is therefore obtained from (24) and (31) in the following manner:

$$\rho\phi = \rho\phi_{\mathrm{mech}} + \rho\phi_{\mathrm{mag}}, \tag{32}$$

which in combination with (18) yields a constitutive relation for stress of the form

$$\sigma = [S_0 + (1-\xi)(S_1-S_0)]^{-1}[\varepsilon - \varepsilon_0(1-\xi)]. \tag{33}$$

The constitutive relation for the magnetization component in the x direction, M, is given by (10) or (19).

V. DEVELOPMENT OF MAGNETIC PARAMETERS

It is proposed that the processes associated with the rotation of magnetization and evolution of domain fraction are reversible. This is because the easy-axis and hard-axis magnetization curves show negligible hysteresis. The easy-axis magnetization process involves evolution of domains, which depends on the magnitude of the magnetostatic energy opposing the external magnetic field, whereas the magnetization along the hard axis is due to magnetization rotation. On the basis of reversible processes, the corresponding driving forces lead to zero increase in entropy. Hence, the driving forces themselves must be zero,

$$\pi^{\theta} = -\frac{\partial(\rho\phi)}{\partial\theta} = 0, \tag{34}$$

$$\pi^{\alpha} = -\frac{\partial(\rho\phi)}{\partial\alpha} = 0. \tag{35}$$

Combination of Eqs. (24), (31), (32), and (34) gives

$$\mu_0 H(1-\xi)M_s\cos\theta - 2K_u(1-\xi)\sin\theta\cos\theta - \mu_0 N M_s^2(2\xi\alpha - \xi + \sin\theta - \xi\sin\theta)(1-\xi)\cos\theta = 0. \tag{36}$$

Ignoring the trivial solutions $\xi=1$ and $\cos\theta=0$, the closed form solution for angle θ is

$$\theta(H,\xi,\alpha) = \arcsin\left(\frac{2\mu_0 N M_s^2\alpha\xi - \mu_0 N M_s^2\xi - \mu_0 H M_s}{\mu_0 N M_s^2\xi - 2K_u - \mu_0 N M_s^2}\right). \tag{37}$$

Similarly, combination of Eqs. (24), (31), (32), and (35) results in

$$2\mu_0 H M_s\xi - \mu_0 N M_s^2(2\xi\alpha - \xi + \sin\theta - \xi\sin\theta) = 0. \tag{38}$$

This yields a closed form solution for domain fraction α,

$$\alpha(H,\xi) = \frac{H}{2NM_s\xi} + \frac{1}{2}. \tag{39}$$

These variables are subject to the constraints $-\pi/2 \leqslant \theta \leqslant \pi/2$ and $0 \leqslant \alpha \leqslant 1$.

The magnetization component in the x direction is obtained from Eqs. (10), (37), and (39),

$$M(H,\xi) = -M_s\left(\frac{4\xi\alpha K_u - 2\xi K_u - \mu_0 M_s\xi H + \mu_0 M_s H}{\mu_0 N M_s^2\xi - 2K_u - \mu_0 N M_s^2}\right). \tag{40}$$

In summary, for a given volume fraction ξ and magnetic field H, the domain fraction α is calculated from Eq. (39). Using this value of α, the magnetization rotation angle θ and magnetization component M are calculated from (37) and (40), respectively. The evolution of ξ is discussed in Sec. VI.

When $\xi \to 1$, it can be seen from Fig. 1 that the material consists of only one variant preferred by field, with the magnetization corresponding to the easy-axis curve. Taking the limit $\xi \to 1$ in (40), one gets

$$M(H)|_{\xi \to 1} = \frac{H}{N}. \tag{41}$$

Conversely, when $\xi \to 0$ the material consists of only one variant preferred by stress with the magnetization corresponding to the hard-axis curve. Taking the limit $\xi \to 0$ in Eq. (40), one gets

$$M(H)|_{\xi \to 0} = \frac{\mu_0 M_s H}{2K_u + \mu_0 N M_s^2}. \tag{42}$$

For comparison of model results with Hall probe measurements,[10] the magnetic induction is calculated by means of the relation

$$B_m = \mu_0 (H + N_x M), \tag{43}$$

where $N_x = 0.434$ is the demagnetization factor in the x direction.[27]

VI. EVOLUTION OF VOLUME FRACTION

A. Mechanical loading

During mechanical loading of the material, the mechanical energy is given by Eq. (31). Therefore, the driving force associated with the evolution of volume fraction has the form

$$\pi^{\xi} = \pi^{\xi}_{\text{mag}} + \pi^{\xi}_{\text{mech}}, \tag{44}$$

with the magnetic and elastic driving forces given by

$$\pi^{\xi}_{\text{mag}} = -\frac{\partial \phi_{\text{mag}}}{\partial \xi} = \mu_0 H M_s (2\alpha - 1 - \sin\theta) + K_u \sin^2\theta - \mu_0 N M_s^2 (2\xi\alpha - \xi + \sin\theta - \xi\sin\theta)(2\alpha - 1 - \sin\theta), \tag{45}$$

$$\pi^{\xi}_{\text{mech}} = -\frac{\partial \phi_{\text{mech}}}{\partial \xi} = -E(\xi)[\varepsilon - \varepsilon_0(1-\xi)]\varepsilon_0 - \frac{1}{2}\frac{\partial E(\xi)}{\partial \xi}[\varepsilon - \varepsilon_0(1-\xi)]^2 + a(\xi)(1-\xi)\varepsilon_0^2 - \frac{1}{2}\frac{\partial a(\xi)}{\partial \xi}\varepsilon_0^2(1-\xi)^2. \tag{46}$$

It is emphasized that if the total driving force is positive, it will assist the evolution of the field-preferred volume fraction ξ, whereas if it is negative, it will oppose it. It will be later seen that the force associated with mechanical driving force remains negative throughout the process, which is evident since the stress always remains compressive indicating that it always opposes the evolution of the field-preferred twin variants.

The start of the detwinning process in shape memory materials and FSMAs requires the overcoming of a finite energy threshold associated with the detwinning stress. This is evident from the stress-strain plots at zero field, and also from strain-field plots.[17,19] Likewise, a finite field strength is required for the evolution of field-preferred variants and ensuing deformation to start. The associated energy or driving force required for twin variant rearrangement to start is estimated from the detwinning stress at zero field. For the Ni–Mn–Ga sample under consideration,[10] the detwinning stress at zero bias field is $\sigma_{\text{tw}} = 0.8$ MPa. The associated critical driving force is calculated as $\pi^{\text{cr}} = \sigma_{\text{tw}}\varepsilon_0 = 46\,400\ \text{J/m}^3$.

From (20), (34), and (35), assuming isothermal process, the Clausius-Duhem inequality is reduced to

$$\pi^{\xi}\dot{\xi} \geqslant 0. \tag{47}$$

During loading, in the initial configuration the sample consists of only one variant preferred by field ($\xi = 1$). The loading process takes place with evolution of stress-preferred variants, $\dot{\xi} \leqslant 0$. The driving force π^{ξ} should therefore be negative in order for inequality (47) to be satisfied. Thus, the increase of stress-preferred volume fraction $(1-\xi)$, or decrease in ξ, begins when the driving force reaches the negative value of the critical driving force. The value of ξ is then obtained by numerically solving the relation

$$\pi^{\xi} = -\pi^{\text{cr}}. \tag{48}$$

Once ξ is determined, the stress σ and magnetization component M are obtained through expressions (33) and (40), respectively. It is noted that ξ is restricted so that $0 \leqslant \xi \leqslant 1$.

B. Mechanical unloading

During unloading, the initial configuration corresponds to the material consisting of one variant preferred by stress ($\xi = 0$, $1-\xi = 1$). This configuration corresponds to a state where the sample is compressed beyond its natural stress-preferred variant length, since the loading is extended even after completion of the detwinning process. Thus, a large negative thermodynamic driving force associated with stress acts on the material along with the driving force associated with the magnetic field, which is always positive. The bias field is present throughout the unloading process.

Since the detwinning strain is given by

$$\varepsilon_{\text{tw}} = \varepsilon_0 \xi, \tag{49}$$

the mechanical energy takes the form

$$\rho\phi_{\text{mech}} = \frac{1}{2}E(\xi)[\varepsilon - \varepsilon_0(1-\xi)]^2 + \frac{1}{2}a(\xi)\varepsilon_0^2\xi^2. \tag{50}$$

The elastic component of the strain is obtained by subtracting the total detwinning strain incurred during loading, ε_0, from the original strain value and then accounting for the detwinning strain given by (49). Thus, the elastic strain has the form

$$\varepsilon_e = \varepsilon - \varepsilon_0 + \varepsilon_{\text{tw}} = \varepsilon - \varepsilon_0 + \varepsilon_0\xi = \varepsilon - \varepsilon_0(1-\xi). \tag{51}$$

Considering energy expression (50), the mechanical component of the driving force has the form

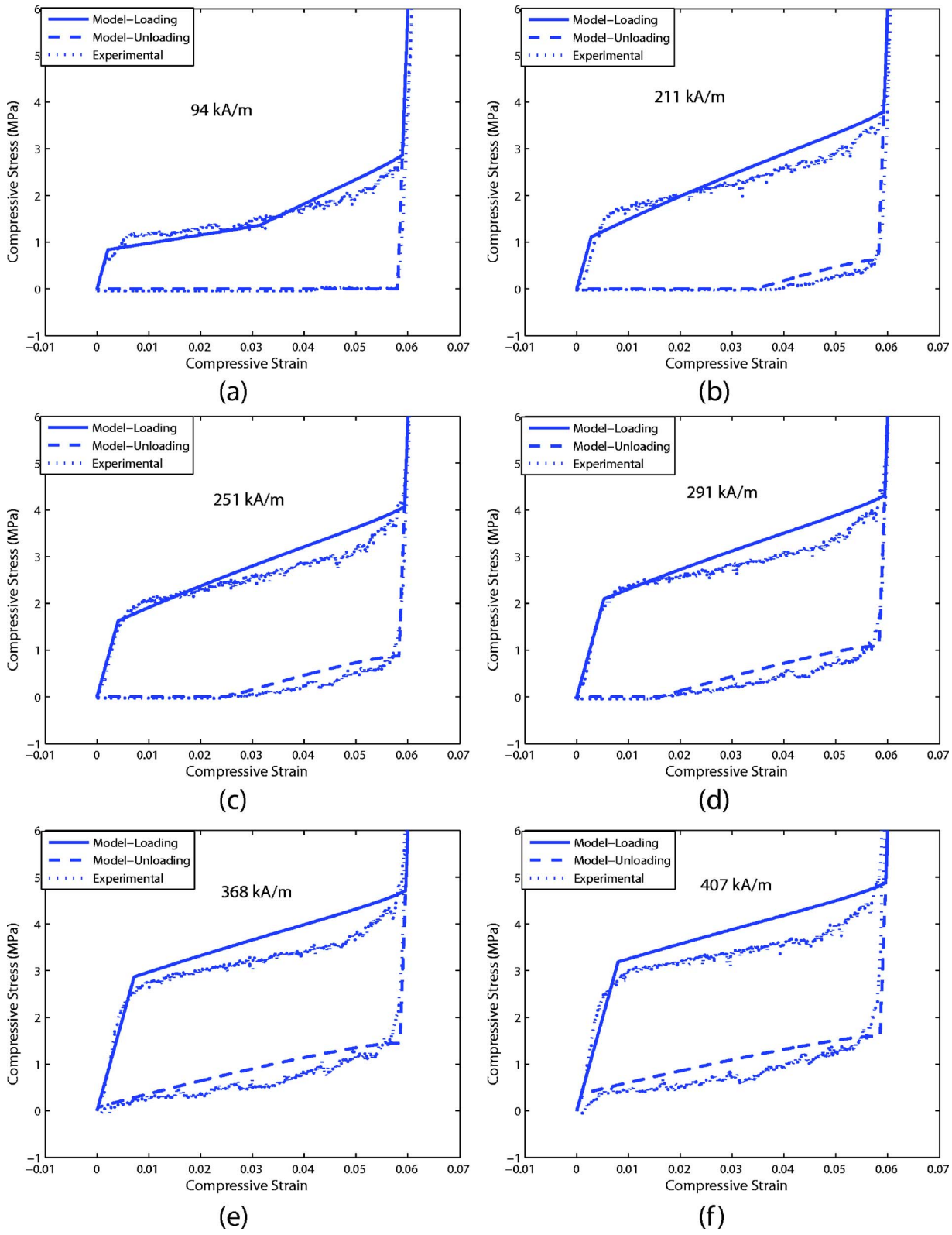

FIG. 3. (Color online) Stress-strain curves at different bias fields. Dotted line: experiment; solid line: calculated (loading); dashed line: calculated (unloading).

$$\pi^{\xi}_{\text{mech}} = -E(\xi)[\varepsilon - \varepsilon_0(1-\xi)]\varepsilon_0 - \frac{1}{2}\frac{\partial E(\xi)}{\partial \xi}[\varepsilon - \varepsilon_0(1-\xi)]^2 - a(\xi)\varepsilon_0^2\xi - \frac{1}{2}\frac{\partial a(\xi)}{\partial \xi}\varepsilon_0^2\xi^2. \tag{52}$$

The unloading process takes place with growth of field-preferred variants, $\dot{\xi} \geqslant 0$. Thus, the total driving force π^{ξ} has to be positive in order for Clausius Duhem inequality (47) to be satisfied. As the total force starts to increase from its lowest negative value, and reaches the positive critical driving force value, the evolution of ξ is initiated. The value of ξ is then found by numerically solving the equation

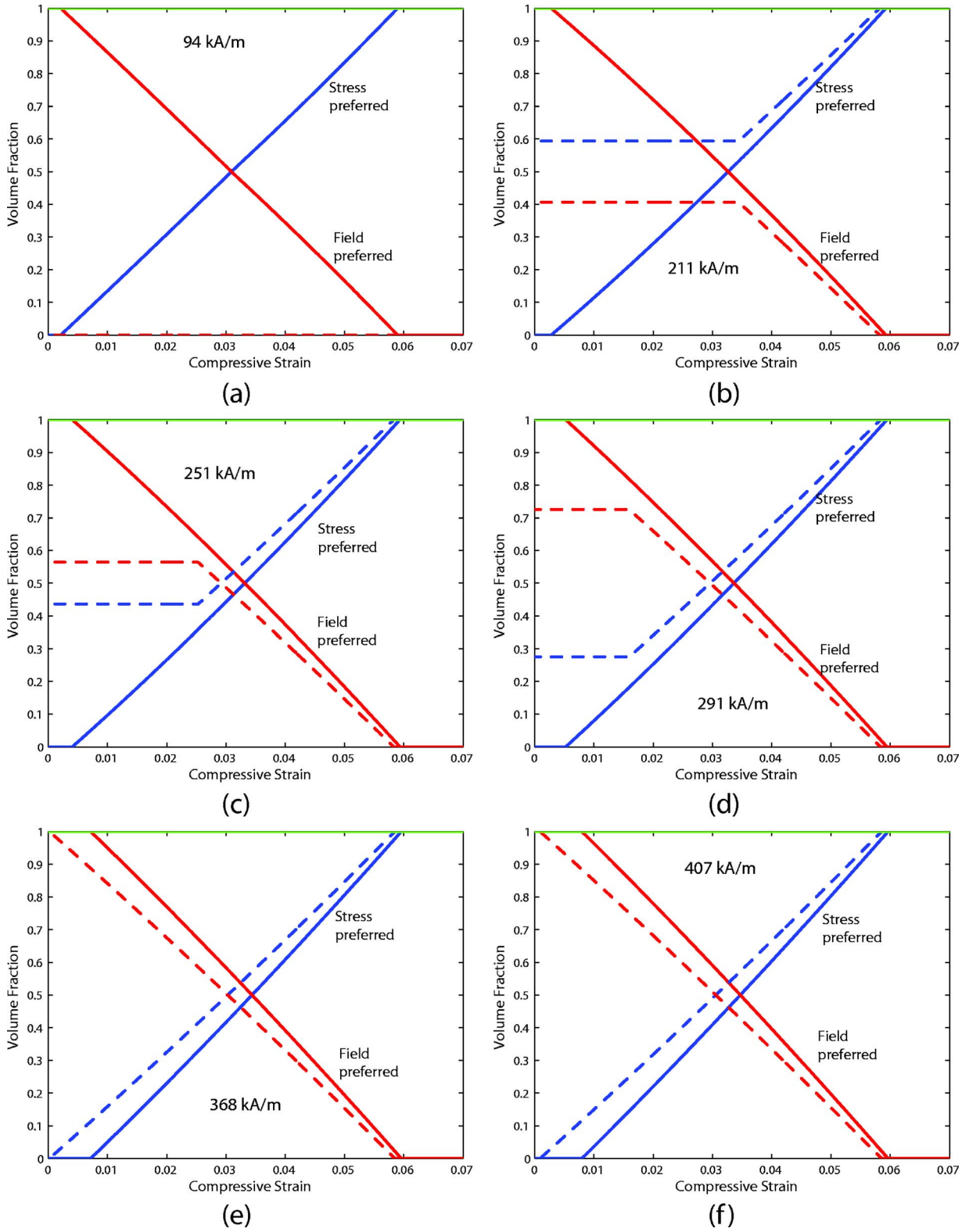

FIG. 4. (Color online) Evolution with increasing compressive strain of field-preferred volume fraction ξ and stress-preferred volume fraction $1-\xi$; solid line: calculated (loading); dashed line: calculated (unloading).

$$\pi^{\xi} = \pi^{\mathrm{cr}}. \tag{53}$$

The constitutive equation for stress, $\sigma = E\varepsilon_e$, has the same form as (33) due to the elastic strain (51) having the same form as (28).

The procedure for arriving at the values of all parameters with a constant bias field and varying strain ε is similar to that outlined earlier. The difference lies in the initial configuration and the terms associated with mechanical energy as stated above. A restriction is placed on the calculated stress that it must always be compressive. Because the sample is

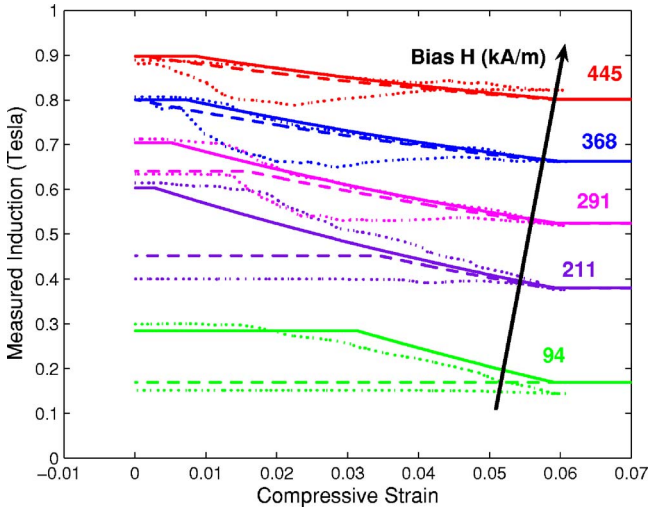

FIG. 5. (Color online) Model results for flux density-strain curves. Dotted line: experiment; solid line: calculated (loading); dashed line: calculated (unloading).

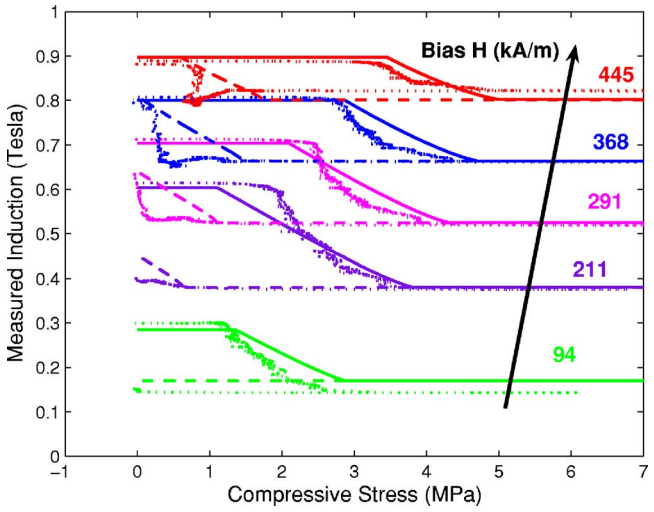

FIG. 6. (Color online) Model results for flux density-stress curves. Dotted line: experiment; solid line: calculated (loading); dashed line: calculated (unloading).

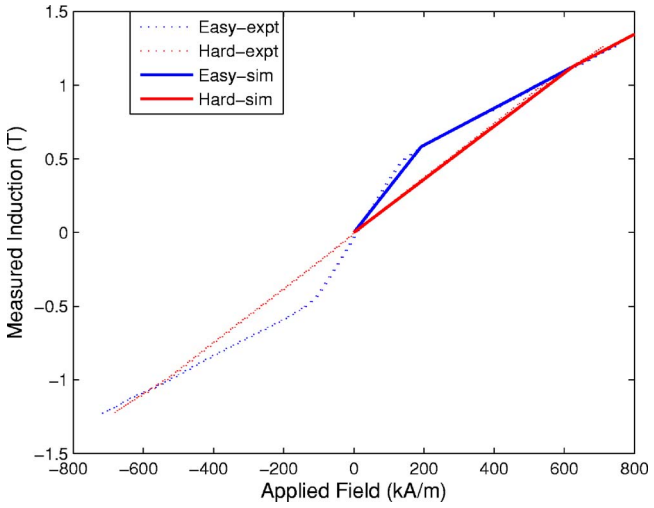

FIG. 7. (Color online) Easy-axis and hard-axis flux density-field curves.

not attached to the test machine's cross arm, no tensile stress is applied to the sample during unloading.

VII. RESULTS AND DISCUSSION

The experimental setup used for model validation and parameter identification consists of an electromagnet and a uniaxial stress stage oriented perpendicular to the axis of the magnetic poles.[10] A $6\times6\times20$ mm^3 single-crystal Ni–Mn–Ga sample (AdaptaMat Ltd.) is placed in the center gap of the electromagnet with its long axis aligned with the stress axis. The sample exhibits a free magnetic-field induced deformation of 5.8% under a field of 720 kA/m. The sample is first converted to a single field-preferred variant by applying a high magnetic field. Then, while being exposed to a bias field, the sample is compressed at a fixed displacement rate of 25.4×10^{-3} mm/s and unloaded at the same rate. This loading and unloading process is repeated for several magnetic bias field intensities ranging between 0 and 445 kA/m. The flux density through the sample is measured by a 1×2 mm^2 transverse Hall probe placed in the gap between one of the magnet poles and a face of the sample. The compressive force is measured by a 200 pounds of force (lbf) load cell, and the displacement is measured by a linear variable differential transducer (LVDT).

Calculated stress-strain plots at bias fields ranging from 94 to 407 kA/m are compared with experimental measurements in Fig. 3. The corresponding evolution of volume fractions ξ and $1-\xi$ is shown in Fig. 4. For the various applied bias fields, the model adequately describes the shape of the hysteresis loop and the amount of pseudoelasticity or residual strain at which the sample returns to zero stress. As the bias field is increased, more energy is required for twin variant rearrangement to start, resulting in an increase in the detwinning stress. In prior models by Likhachev and Ullakko[14] and Straka and Heckzo,[6] a term known as "magnetic field induced stress" was introduced to account for this effect. Our model requires no adjustments. The field-induced stress was accurately calculated by Chernenko *et al.*;[13] the magnetoelastic coupling was proposed as the origin of field-induced stress.

Our model accurately quantifies the monotonic increase in detwinning stress with increasing bias field for fields above 195 kA/m; the detwinning stress remains constant at lower field values. This behavior occurs because the driving force due to magnetic field (45) remains zero for fields lower than 195 kA/m, when $\xi=1$. At low field values, during the start of the compression the magnetic field creates no opposition to twin boundary motion. This creates a discontinuity in the stress-strain plot when the driving force due to magnetic field becomes nonzero; see 94 kA/m case in Fig. 3.

The flux density plots shown in Figures 5 and 6 are of interest for sensing applications. The absolute value of flux density decreases with increasing compressive stress. As the sample is compressed from its initial field-preferred variant state, the stress-preferred variants grow at the expense of field-preferred variants. Due to the high magnetocrystalline anisotropy of Ni–Mn–Ga, the nucleation and growth of stress-preferred variants occurs in concert with the rotation

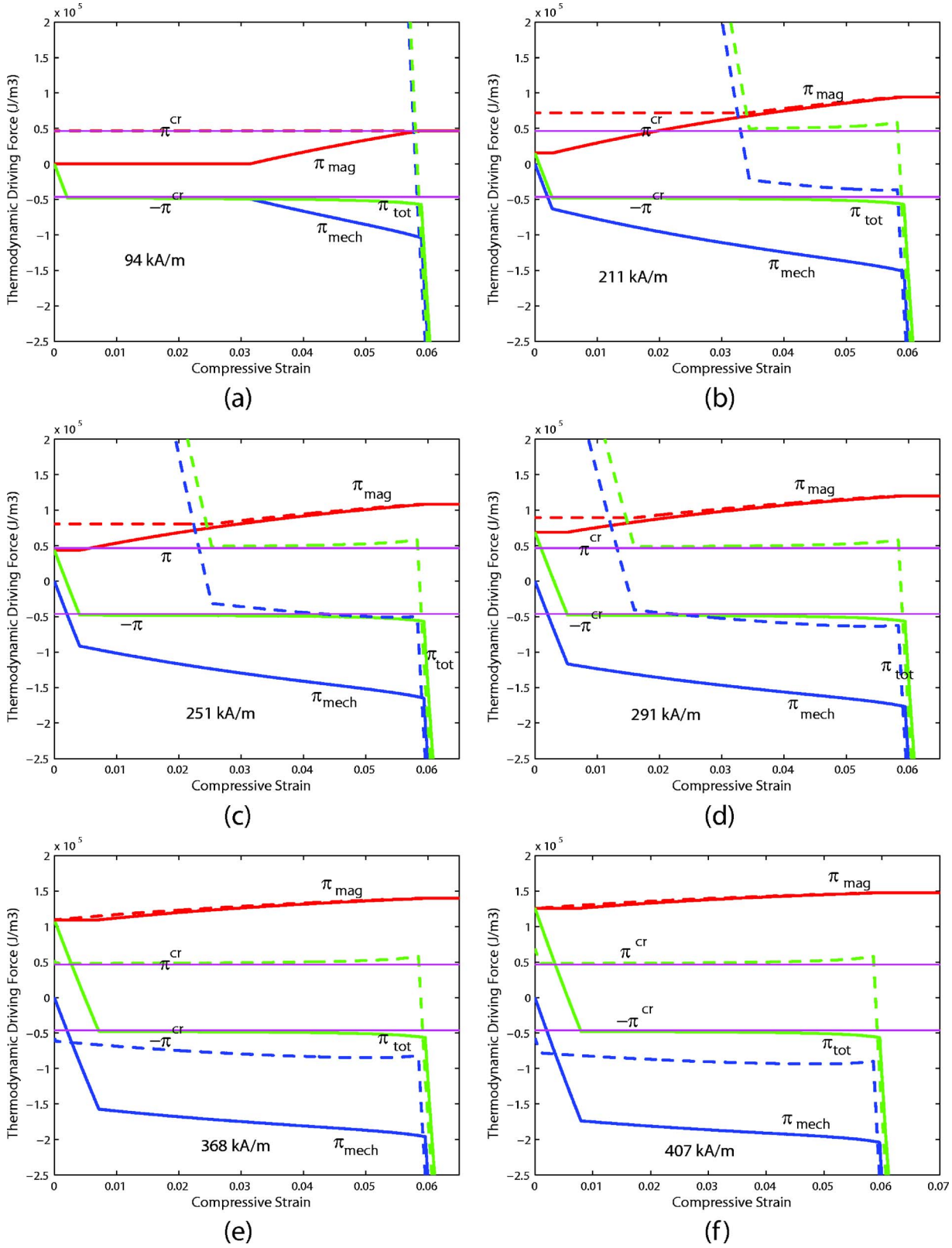

FIG. 8. (Color online) Evolution of thermodynamic driving forces with increasing compressive strain at different bias fields. Solid line: calculated (loading); dashed line: calculated (unloading).

of magnetization vectors into the longitudinal direction, which causes a reduction of the permeability and flux density in the transverse direction. There is a strong correlation between Figs. 3, 5, and 6 regarding the reversibility of the magnetic and mechanical behaviors. Because a change in flux density relative to the initial field-preferred single variant is directly associated with the growth of stress-preferred variants, the flux density value returns to its initial value only if the stress-strain curve exhibits magnetic field induced pseudoelasticity. The model calculations accurately reflect

this trend. Furthermore, the model correctly identifies the transition from irreversible quasiplastic to reversible pseudoelastic behavior at a bias field of 368 kA/m. The simulated curves in Fig. 5 show less hysteresis than the measurements and a slight nonlinearity in the relationship between flux density and strain. This is in agreement with measurements by Straka and Heckzo[28] in which the magnetization varies in a nonlinear and hysteretic fashion with strain, and contrary to prior models which postulate linear dependence of strain on magnetization.[7,14] As shown in Fig. 6, the model accurately quantifies the dependence of flux density on stress. While the tests were conducted in displacement control, the observed trends should resemble those obtained experimentally with stress as the independent variable. The easy-axis and hard-axis magnetization curves obtained through Eqs. (41) and (42) match the experimental data, as shown in Fig. 7.

The evolution of the thermodynamic driving forces acting on a twin boundary with increasing compressive strain is shown in Fig. 8. It is seen that the driving force due to stress is always negative since the stress is always compressive, and more importantly, it always opposes the growth of field volume fraction ξ. In addition, the driving force due to magnetic field is always positive indicating that the field always favors the growth of volume fraction ξ. During loading, the total force has to overcome the negative critical driving force $(-\pi^{cr})$ for twin variant rearrangement to start. Similarly, during unloading, the total force has to overcome the positive critical driving force (π^{cr}) for the start of twin variant rearrangement in the opposite direction. The magnitudes of total driving force during twin variant rearrangement for loading and unloading are negative and positive, respectively, in order to satisfy Clausius-Duhem inequality (47). Once the twin boundary motion is initiated, the total driving force remains at almost the same value as the critical driving force value. It is also observed that the strain at which the driving force due to stress becomes positive is the same strain at which the sample stops expanding, and is the same strain corresponding to the partial pseudoelasticity.

VIII. CONCLUDING REMARKS

A thermodynamic model for the sensing effect in Ni–Mn–Ga is presented. The model is low order and requires only seven parameters which are identified from simple magnetomechanical measurements: stress-strain plot at zero magnetic field, and easy-axis and hard-axis magnetization curves. The magnetic parameters include saturation magnetization M_s, anisotropy constant K_u, and demagnetization factor N; the former two parameters can be obtained from the easy-axis and hard-axis magnetization curves, the latter from the sample geometry. All the parameters related to mechanical energy are determined from the stress-strain plot at zero magnetic field. These include the detwinning stress at zero field σ_{tw}, the elastic modulus during start and end of compression, E_0 and E_1, respectively, and the slope over the detwinning region k. The lattice distortion ε_0 is a property of the crystal.

In concert with the required experimental measurements, the model can be used for design and control of a Ni–Mn–Ga displacement sensor. At a bias field of 368 kA/m, the sensor produces a reversible flux density change of 145 mT over a range of 5.8% strain and 4.4 MPa stress. By way of comparison, Terfenol-D can produce a higher maximum sensitivity of 0.4 T at a lower field of 16 kA/m and higher stress range of 20 MPa. However, the associated deformation range is only 0.1% due to the higher Terfenol-D stiffness.

ACKNOWLEDGMENT

We acknowledge the financial support of National Science Foundation through Grant CMS-0409512.

[1] S. J. Murray, M. Marioni, S. M. Allen, R. C. O'Handley, and T. A. Lograsso, Appl. Phys. Lett. **77**, 886 (2000).
[2] C. P. Henry, D. Bono, J. Feuchtwanger, S. M. Allen, and R. C. O'Handley, J. Appl. Phys. **91**, 7810 (2002).
[3] O. Soderberg, Y. Ge, A. Sozinov, S. Hannula, and V. K. Lindroos, Smart Mater. Struct. **14**, S223 (2005).
[4] J. Kiang and L. Tong, J. Magn. Magn. Mater. **292**, 394 (2005).
[5] P. Mullner, V. A. Chernenko, and G. Kostorz, Scr. Mater. **49**, 129 (2003).
[6] L. Straka and O. Heczko, IEEE Trans. Magn. **39**, 3402 (2003).
[7] O. Heczko, J. Magn. Magn. Mater. **290–291**, 787 (2005).
[8] G. Li, Y. Liu, and B. Ngoi, Scr. Mater. **53**, 829 (2005).
[9] I. Suorsa, E. Pagounis, and K. Ullakko, Appl. Phys. Lett. **84**, 4658 (2004).
[10] N. Sarawate and M. Dapino, Appl. Phys. Lett. **88**, 121923 (2006).
[11] R. C. O'Handley, J. Appl. Phys. **83**, 3263 (1998).
[12] N. I. Glatavaska, A. A. Rudenko, I. N. Glavatskiy, and V. A. L'vov, J. Magn. Magn. Mater. **265**, 142 (2003).
[13] V. A. Chernenko, V. A. L'vov, P. Mullner, G. Kostorz, and T. Takagi, Phys. Rev. B **69**, 134410 (2004).
[14] A. A. Likhachev and K. Ullakko, Phys. Lett. A **275**, 142 (2000).
[15] R. N. Couch and I. Chopra, Proc. SPIE **5764**, 1 (2005).
[16] L. C. Brinson, J. Intell. Mater. Syst. Struct. **4**, 229 (1993).
[17] L. Hirsinger and C. Lexcellent, J. Phys. IV **112**, 977 (2003).
[18] L. Hirsinger, Phys. Status Solidi C **1**, 3458 (2004).
[19] B. Kiefer and D. C. Lagoudas, Philos. Mag. **85**, 4289 (2005).
[20] L. E. Faidley, M. J. Dapino, G. N. Washington, and T. A. Lograsso, Proc. SPIE **5761**, 501 (2005).
[21] A. Malla, M. Dapino, T. Lograsso, and D. Schlagel, J. Appl. Phys. **99**, 063903 (2006).
[22] Y. H. Pao and K. Hutter, Proc. IEEE **63**, 1011 (1975).
[23] Y. Ge, O. Heczko, O. Soderberg, and V. K. Lindroos, J. Appl. Phys. **96**, 2159 (2004).
[24] V. A. L'vov, S. P. Zagorodnyuk, and V. A. Chernenko, Eur. Phys. J. B **27**, 55 (2002).
[25] R. C. O'Handley, *Modern Magnetic Materials: Principles and Applications* (Wiley-Interscience, United States, 2000).
[26] E. Patoor, D. C. Lagoudas, P. B. Entchev, L. C. Brinson, and X. Gao, Mech. Mater. **38**, 391 (2006).
[27] D. C. Jiles, *Introduction to Magnetism and Magnetic Materials* (Chapman & Hall, London, 1998).
[28] L. Straka and O. Heczko, Scr. Mater. **54**, 1549 (2006).